Electronic Supplementary Material (ESI) for Journal of Materials Chemistry C.

Supplementary Information for "Self-assembled non-volatile micro memory arrays of molecular ferroelectrics"

Yichen Cai[a‡], Muhammad Zaheer[a‡], Wei Jin[a], Jiao Wang[a], Yabing Shan[a], Qingmiao Nie[b*], Wenchong Wang[c], Mengge Yan[d], Bobo Tian[d], Chunxiao Cong[a], Zhi-Jun Qiu[a], Ran Liu[a*], Lirong Zheng [a] and Laigui Hu[a*]

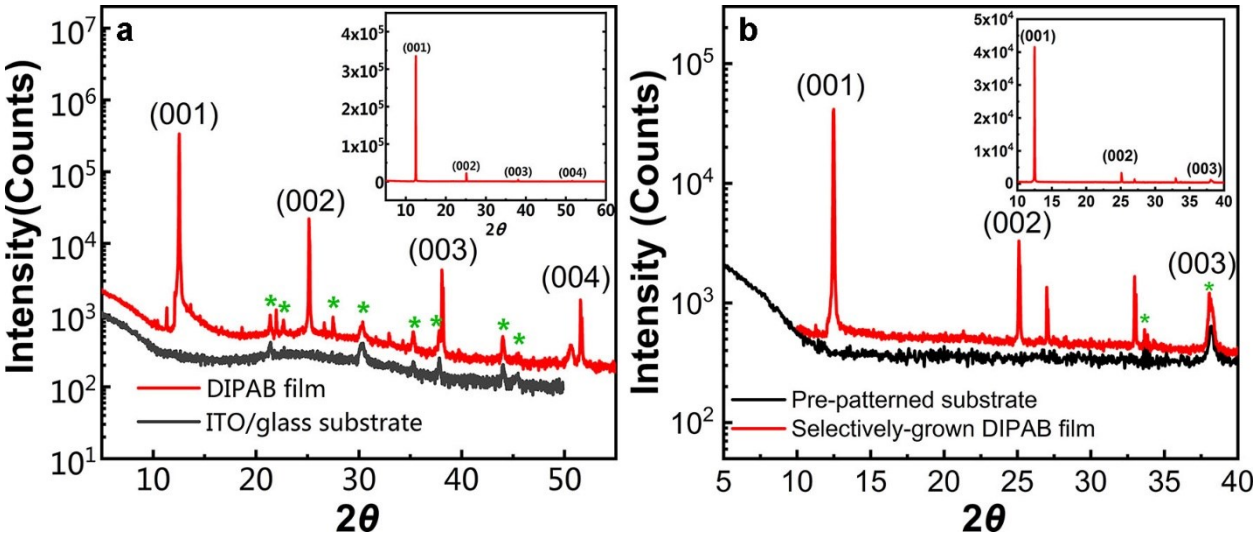

Fig. S1 XRD patterns (semi-log scale) of the DIPAB films (red line) and substrates (black line). (a) XRD patterns of continuous films on ITO/glass substrates. Inset is the patterns plotted in a linear scale. (b) XRD patterns of area-selectively grown films on patterned substrates. nset is the patterns plotted in a linear scale.

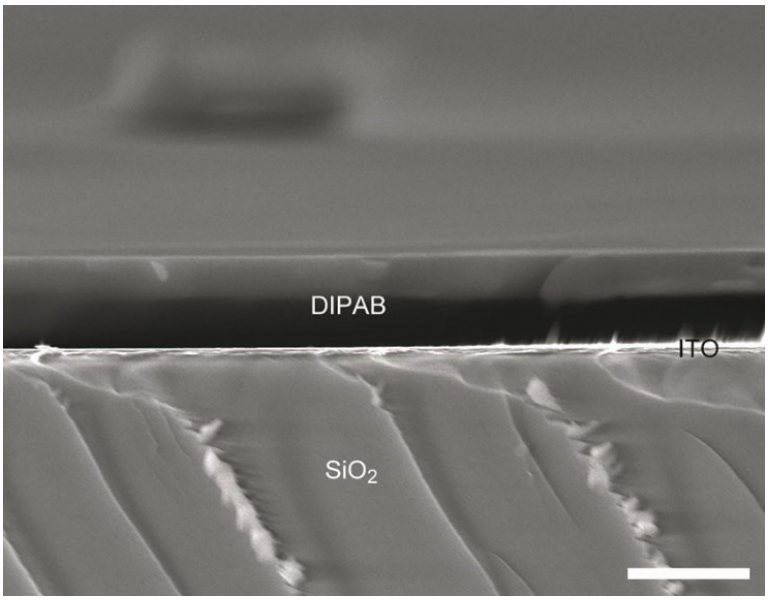

Fig. S2 Cross-sectional SEM image of the DIPAB films. Scale bar is 1 μm.

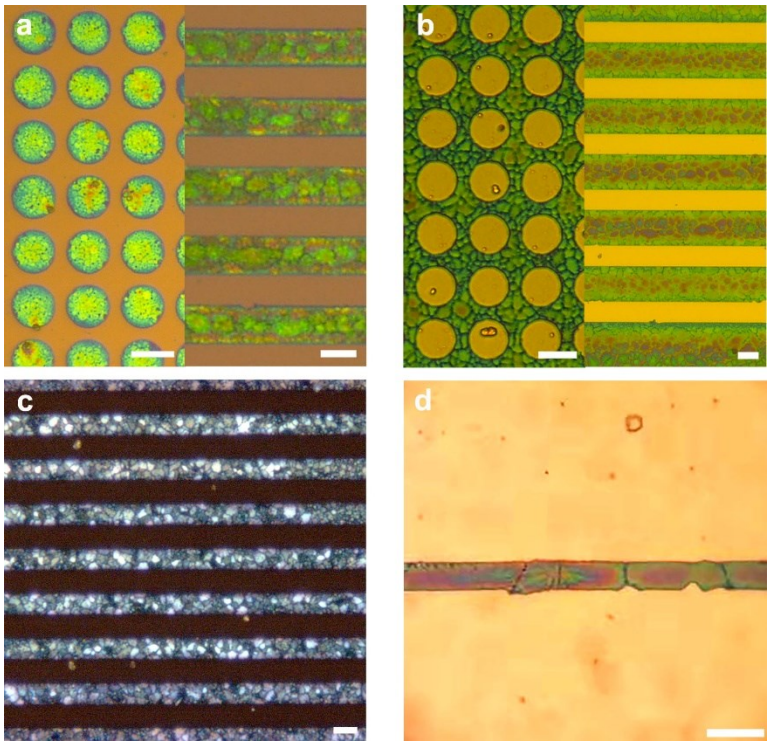

Fig. S3 Area-selective solution growth of CA films. (a) CA films grown on the patterned Au electrodes. (b) CA films grown in the electrode gaps. (c) POM images of the CA films in the electrode gaps, which shows highly-crystalline films with large crystallites. (d) CA films in a narrow 5-μm electrode gap. Scale bars are 10 μm.

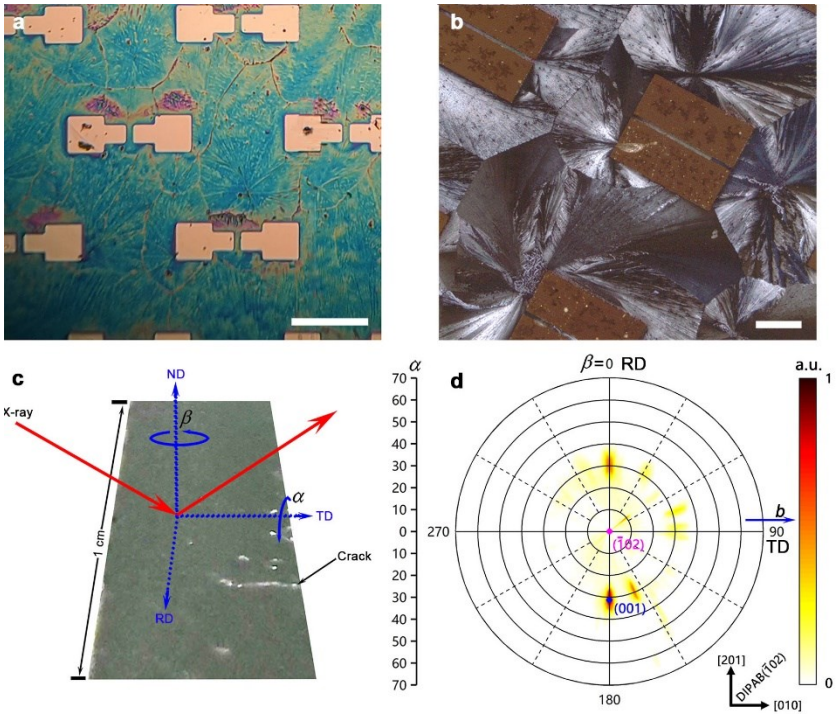

Fig. S4 Spherocrystal structures in large electrode gaps with area-selectively grown films and large-area electrodes for the convenience of characterization. (a) Optical microscope images. (b) POM image. The large area of the electrodes can lead to the formation of isolated islands on the electrodes. The scale bars are 200 μm. (c) Photograph of a uniform DIPAB film on SiO_2/Si with a size of ~ 1 × 0.5 cm^2 and a few cracks, which is a part of a larger wafer-scale film with more cracks. All the cracks are along the texture lines of DIPAB films. ($\bar{1}02$) pole figure was collected with the projection of the incident X-ray on the film surface initially along the TD direction. Then the substrate was rotated azimuthally from 0° to 360° (β) at a series of tilt angles α from 0° to 70° with a step of 2.5°. (d) The ($\bar{1}02$) pole figure of DIPAB film with the (001) diffraction spot indicates that the as-prepared DIPAB films have both out-of-plane orientation and in-plane certain orientation [18]. Based on the crystal structure, the intersection of the (001) plane and the ($\bar{1}02$) plane is the *b*-axis [010], indicating that the *b*-axis has to be along the TD direction as well as along the texture lines.

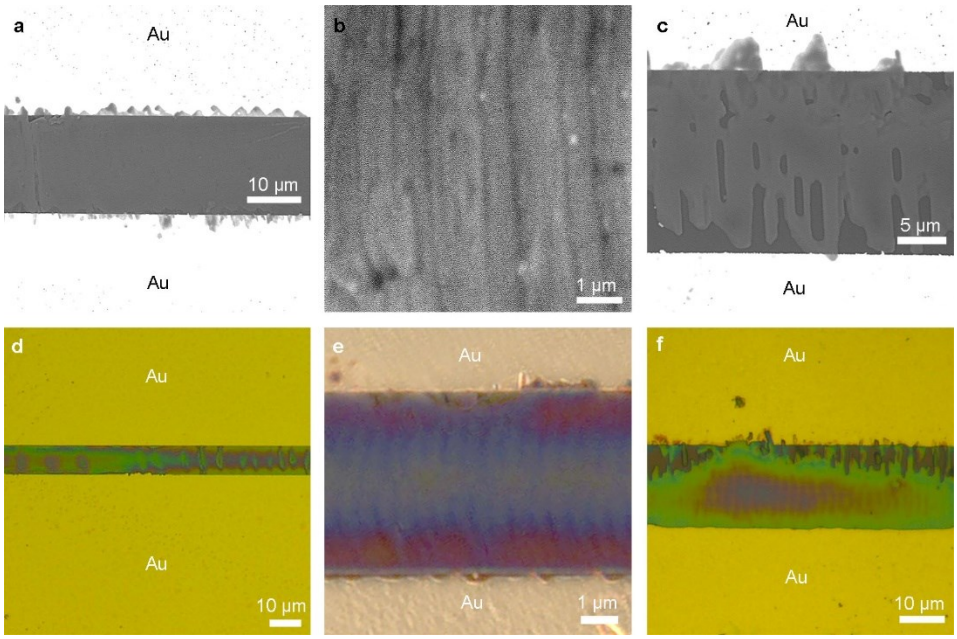

Fig. S5 Texture lines of the area selective grown films in narrow gaps. (a) SEM image of the DIPAB film in a narrow electrode gap. (b) Magnified image of Fig. S5a. Texture lines can be clearly observed. (c) SEM image of discontinuous DIPAB films which are intentionally produced as an intermediate state before the formation of continuous films. (d) Optical microscope image of the sample in Fig. S5a. (e) POM image. (f) Optical microscope image for intermediate-state films. As shown in Fig. S5, the films in the gaps mainly stem from one side of the electrode gap, producing adjacent micro/nano belts along the growth direction with the resultant texture lines. This confirms that the DIPAB crystals have the tendency to grow along the polar *b*-axis.

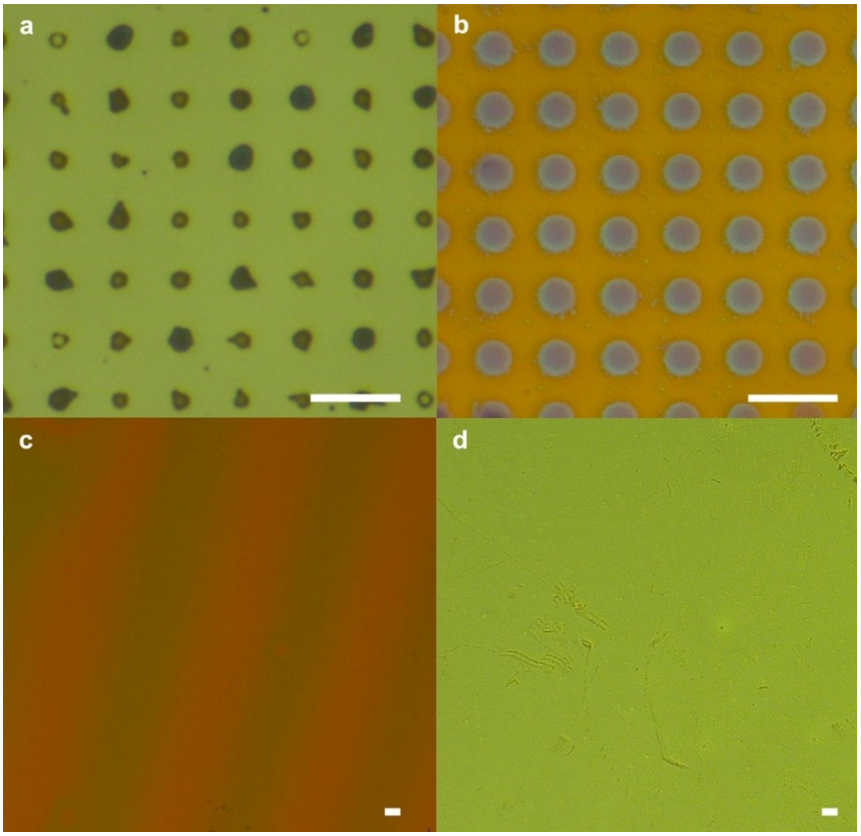

Fig. S6 Area-selective growth for other organic materials. (a) Rubrene films on patterned Au electrodes. (b) Tris-(8-hydroxyquinoline) aluminum (Alq_3) films on patterned Au electrodes. (c) Continuous rubrene films. (d) Continuous Alq_3 films. The scale bars are 10 μm.

Table S1 Comparison of different ferroelectrics

Type	Material	E_c (kV cm^{-1})	P_s (μC cm^{-2})	T_c (K)	Refference
	DIPAB device array	**5-15**	**~20 (P_r)**	**-**	**This work**
	CA	11-29	30 [S12]	> 400	[S1]
	DIPAC	9	8.9	440	[S2]
	MBI	>11	5-10	> 400	[S3]
	DIPAB	5	23	426	[S4]
Molecular ferroelectrics	(benzylammonium)$_2$PbCl$_4$	10-13	13	438	[S5]
	[Hdabco]BF$_4$	15-30	~5	-	[S6]
	TMCM-MnCl$_3$	-	4	406	[S7]
	HQReO$_4$	2-5	～4 (345 K)	367	[S8]
	MDABCO-NH$_4$I$_3$	6-12	22	448	[S9]
	TMCM-CdBr$_3$	-	3.5	346	[S10]
	[3-O-Q]ClO$_4$	-	6.7	457	[S11]
Polymer ferroelectrics	P(VDF-TrFE)	～500	～8	363	[S14]
	Nylon-11	600	5	-	[S14]
Inorganic ferroelectrics	PZT	20-80	30-50	-	[S13]
	BTO	10	26	381	[S14]

Note: Most data of the MF materials are obtained from crystals, instead of thin film devices.

References

[S1] Horiuchi S, Tokunaga Y, Giovannetti G, et al. Above-room-temperature Ferroelectricity in a Single-component Molecular Crystal. Nature, 2010, 463(7282), 789-792.

[S2] Fu D W, Zhang W, Cai H L, et al. Diisopropylammonium Chloride: A Ferroelectric Organic Salt with a High Phase Transition Temperature and Practical Utilization Level of Spontaneous Polarization. Advanced Materials, 2011, 23(47), 5658-5662.

[S3] Horiuchi S, Kagawa F, Hatahara K, et al. Above-room-temperature Ferroelectricity and Antiferroelectricity in Benzimidazoles. Nature Communications, 2012, 3, 1308.

[S4] Fu D W, Cai H L, Liu Y, et al. Diisopropylammonium Bromide Is a High-Temperature Molecular Ferroelectric Crystal. Science, 2013, 339(6118), 425-428.

[S5] Liao W Q, Zhang Y, Hu C L, et al. A Lead-halide Perovskite Molecular Ferroelectric Semiconductor. Nature Communications, 2015, 6, 7338.

[S6] Shi P P, Tang Y Y, Li P F, et al. De Novo Discovery of [Hdabco]BF_4 Molecular Ferroelectric Thin Film for Nonvolatile Low-Voltage Memories. Journal of the American Chemical Society, 2017, 139(3), 1319-1324.

[S7] You Y M, Liao W Q, Zhao D W, et al. An Organic-inorganic Perovskite Ferroelectric with Large Piezoelectric Response. Science, 2017, 357(6348), 306-309.

[S8] Harada J, Shimojo T, Oyamaguchi H, et al. Directionally Tunable and Mechanically Deformable Ferroelectric Crystals from Rotating Polar Globular Ionic Molecules. Nature Chemistry, 2016, 8, 946-952.

[S9] Ye H Y, Tang Y Y, Li P F, et al. Metal-free Three-dimensional Perovskite Ferroelectrics. Science 2018, 361(6398), 151-155.

[S10] Liao W Q, Tang Y Y, Li P F, et al. The Competitive Halogen Bond in the Molecular Ferroelectric with Large Piezoelectric Response. Journal of the American Chemical Society, 2018, 140(11), 3975.

[S11] Yang C K, Chen W N, Ding Y T, et al. Directional Intermolecular Interactions for Precise Molecular Design of a High T_c Multiaxial Molecular Ferroelectric. Journal of the American Chemical Society, 2019, 141(4), 1781-1787.

[S12] Horiuchi S, Kobayashi K, Kumai R, et al. Proton Tautomerism for Strong Polarization Switching. Nature Communications, 2017, 8, 14426.

[S13] Foster C M, Bai G R, Csencsits R, et al. Single-crystal $Pb(Zr_xTi_{1-x})O_3$ Thin Films Prepared by Metal-organic Chemical Vapor Deposition: Systematic Compositional Variation of Electronic and Optical Properties. Journal of Applied Physics, 1997, 81(5), 2349-2357.

[S14] Horiuchi S, Tokura Y. Organic Ferroelectrics. Nature Materials, 2008, 7(5), 357-366.